Vol. 7 No. 1 (2024) 43 – 57 | doi.org/10.33116/ije.v7i1.186

IJE | INDONESIAN JOURNAL OF ENERGY
P-ISSN: 2549-1016 | E-ISSN: 2549-760X
available online at www.ije-pyc.org

Published by: The Purnomo Yusgiantoro Center

Estimations of the Geothermal Energy Potential in The Mount Anak Krakatau Region Based on Derivative Analysis and 3D Model of Gravitational Satellite Data

Nanda R. Permana [1,*], Belista Gunawan [2]

[1] PT Minelog Services Indonesia, Industrial Estate and Warehouse Techno Park Block G1 Number 10, Banten 15220, Indonesia.
[2] GeoXplore Indonesia, Kincir Air Street, Pondok Manggis Block B6, Bogor 16920, Indonesia.

*Corresponding Author: nandaridki836@gmail.com

Article History

Received 9 October 2023
Accepted 15 February 2024
Available 28 February 2024

Abstract

Geothermal energy is a source of renewable energy that has the potential to be produced, considering that Indonesia is in the ring of fire, where there are many volcanoes, one of which is Mount Anak Krakatau. Even though direct exploration is not permitted, at least information on the geothermal system on the mountain can still be obtained using satellite data. Therefore, this study aims to analyze the geothermal energy potential of Mount Anak Krakatau using gravity satellite data with a total of 320 data consisting of gravity disturbance, geoid, and Digital Elevation Model. The data processing describes a 3D model that is correlated with the First Horizontal Derivative (FHD) and Second Vertical Derivative (SVD) analysis. Based on the results of the residual anomaly map analysis, the low anomaly has a value of -1.85–(-0.89) mGal which is suspected to be associated with magma pockets, and the high anomaly ranges from 0.04–2.13 mGal which is suspected to be associated with the caldera of Mount Anak Krakatau. Based on the results of the FHD and SVD graphical analysis, there are 18 faults that control the geothermal system. Based on the results of 3D modeling trending from west-east it can be seen that there is a clay cap layer with a value density 2.32–2.37 gr/cc at depths of 0–550 m and reservoir layers with density values of 2.23–2.29 gr/cc at depths of 500–1100 m. This geothermal research using the gravity method can be developed and become a reference for future research to calculate the potential for electrification in a research area.

Keywords:
derivative analysis, geothermal potential, gravity method, 3D inversion model, Mount Anak Krakatau

1. Introduction

Indonesia possesses geothermal energy reserves of approximately 29 GWe, which is about 40% of the world's total reserves. The geothermal energy potential of Indonesia is the second-largest after the United States (Dewi et al, 2015). Furthermore, Indonesia possesses numerous volcanoes, earning its classification among the world's active volcanoes situated in The Ring of Fire (Citraningrum et al., 2023). Therefore, geothermal energy has become a highly promising renewable alternative energy source for production in Indonesia. One of the geothermal areas that can be optimized for electrification is Mount Anak Krakatau, which is an active volcano. While it may not be feasible to construct a power plant in the vicinity of the area, at least information regarding the geothermal potential from Mount Anak Krakatau is necessary.

According to previous research on identifying the magma body of Mount Anak Krakatau based on the 3D seismic velocity structure using local earthquake tomography, there exists a magma spatial structure beneath the Krakatau complex, situated at depths of 3–5 km. The presence of this zone is evidenced by a relatively low P-wave velocity anomaly and an extremely low S-wave velocity anomaly, as well as a high Vp/Vs ratio (Syafawi et al., 2015). As a form of research development, this study, therefore, employs a different method aiming to analyze the geothermal energy potential in the Mount Anak Krakatau region based on derivative analysis and 3D modeling of gravitational satellite data.

Geothermal energy is the energy stored in the form of hot water or steam at specific geological conditions and depths deep within the Earth's crust (Ramadhan et al., 2020). This energy can be accessed as groundwater transfers heat from rocks to the surface through boreholes or natural cracks and faults (Sigfússon and Uihlein, 2015). The geothermal system consists of three main elements: a heat source, a reservoir for heat accumulation, and a cap rock to maintain the heat accumulation (Figure 1) (Firdaus et al., 2014). One crucial factor in a geothermal system is the existence of a reservoir. This reservoir is a layer containing hot fluids beneath the surface that is associated with rocks having higher density, contrasting with the surrounding rocks. This density contrast can be observed from gravitational data, which shows anomalies in the gravity map (Raharjo et al., 2022).

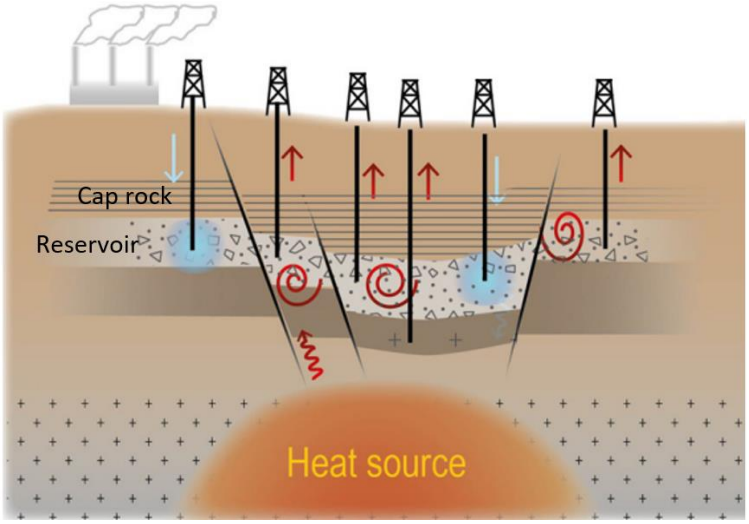

Figure 1. Geothermal system (Buijze et al, 2019).

The gravity method is a geophysical exploration technique that is based on variations in mass density below the earth's surface (Nafian et al., 2021). In geothermal energy exploration, the gravity method can detect differences in rock density beneath the surface that form a geothermal system (Rizkiani & Rustadi, 2019). The gravity method uses the principle of Newton's law of gravity, which explains that two particles with masses $m1$ and $m2$ have an attractive force proportional to the product of their masses and inversely proportional to the square of the distance between their centers of mass, as shown in the equation (Telford et al., 2004):

$$\vec{F}(r) = G\frac{m_1 m_2}{R^2}\hat{r} \quad (1)$$

In the gravity method, there are gravity corrections that need to be performed to obtain more accurate results from satellite gravity data. Among these corrections are Bouguer and Terrain corrections. The Bouguer correction accounts for variations in the gravitational pull of rock masses on the earth's surface and can be calculated from the derived data (Rachmawati et al., 2019). Terrain correction occurs due to geographical elements within the survey area, where variations in elevation, such as hills and valleys surrounding the measurement site, influence the measurements. (Gunawan et al., 2022).

The examination of gravity data derivatives is employed to detect geological formations, incorporating the First Horizontal Derivative (FHD) and Second Vertical Derivative (SVD). These derivatives act as

low-pass filters, effectively isolating low-frequency and high-frequency components (Raharjo et al., 2022).

$$\mathrm{FHD} = \sqrt{\left(\frac{\partial \mathrm{g}}{\partial \mathrm{x}}\right)^2 + \left(\frac{\partial \mathrm{g}}{\partial y}\right)^2} \tag{2}$$

The First Horizontal Derivative (FHD) is utilized to determine the location of horizontal density contrast boundaries from gravity data (Cordell, 1979). Changes in the anomaly horizontally are characterized by the maximum value of FHD in the FHD plot. Therefore, the maximum value of FHD represents geological fault features. The value of FHD can be obtained from Equation 2.

The Second Vertical Derivative (SVD) functions as a high-pass filter, enhancing the near-surface effects and disregarding deeper anomalies. Therefore, the results obtained are associated with shallow structures (Fitriani et al., 2020). Since the gravity field satisfies the Laplace equation, the SVD can be obtained from horizontal derivatives.

$$\frac{\partial^2 g}{\partial z^2} = \left(\frac{\partial^2 g}{\partial x^2} + \frac{\partial^2 g}{\partial y^2}\right) \tag{3}$$

SVD can be used to identify the type of fault, whether it is a normal fault or a reverse fault. The criteria for determining the type of fault are as follows (Aufia et al., 2019).

$$\left(\frac{\partial^2 g}{\partial z^2}\right)_{maks} > \left|\left(\frac{\partial^2 g}{\partial z^2}\right)\right|_{min} = \text{Normal Fault} \tag{4}$$

$$\left(\frac{\partial^2 g}{\partial z^2}\right)_{maks} < \left|\left(\frac{\partial^2 g}{\partial z^2}\right)\right|_{min} = \text{Reverse Fault} \tag{5}$$

According to the Ministry of Energy and Mineral Resources (ESDM), astronomically, Mount Anak Krakatau is located at 6° 6' 5.8" S and 105° 25' 22.3" E. Geographically, it is situated in the Sunda Strait, South Lampung Regency, Lampung Province. Based on field observations, the research area can generally be divided into two geomorphological units: the hilly intrusion landform unit and the coastal plain landform unit (Putra & Yulianto, 2017). This volcano, located in the Sunda Strait, has a history of impactful eruptions, including tsunamis in 1883 and 2018 (Perwita et al., 2020).

Mount Anak Krakatau is a volcanic island featuring a single active cone located in the center of its caldera. This cone experiences eruptions at intervals ranging from 1 to 8 years and exhibits Strombolian and Vulcanian eruption characteristics (Ariyanti & Fattah, 2020). Mount Anak Krakatau is composed of alternating eruption materials, such as pyroclastic fall, pyroclastic flow, and lava flow deposits (Sumintadireja, 2012). These layers have formed a cone that currently reaches a height of 315 meters. The Krakatau Volcanic Complex consists of four islands: Rakata, Sertung, Panjang, and Anak Krakatau (Figure 2) (Sutawidjaja, 2006). Tectonic movements related to the South Sumatra Fault System significantly impact the Krakatau Volcanic Complex (Saad, 2022). The tectonic extensional characteristics in this zone are characterized by fault blocks in the bedrock, active normal faults, the formation of graben morphology, and crustal thinning (Tim Badan Geologi, 2019).

2. Method

The research location is situated at Mount Anak Krakatau, Lampung, with predefined boundaries covering an area of 15.5 km^2, as shown in Figure 3. The gravity anomaly data consists of gravity disturbance (gd), geoid, and Digital Elevation Model (DEM) obtained from the Bureau Gravimetrique International (GGMplus 2013) and Murray Lab Caltech GGMplus 2013 websites, comprising a total of 320 data points. GGMPlus is a gravity field model based on GRACE (ITG2010) satellite data, GOCE satellite (TIM-4), EGM2008, and gravity topography. GGMplus provides an updated representation of Earth's gravity, incorporating information on gravity acceleration, radial and horizontal field

components, and quasi-geoid heights. This detailed depiction involves a vast dataset exceeding 3 billion points, encompassing 80% of Earth's landmass within the ± 60° latitude range (Suprianto et al., 2021). The data resolution of GGMPlus is approximately 200 meters (Hirt et al., 2013). The primary limitation of the GGMplus model remains its constrained coverage, as it provides data only up to a distance of 10 kilometers from the coastline (Camacho & Alvarez, 2021), when compared to measurements on land using a gravimeter.

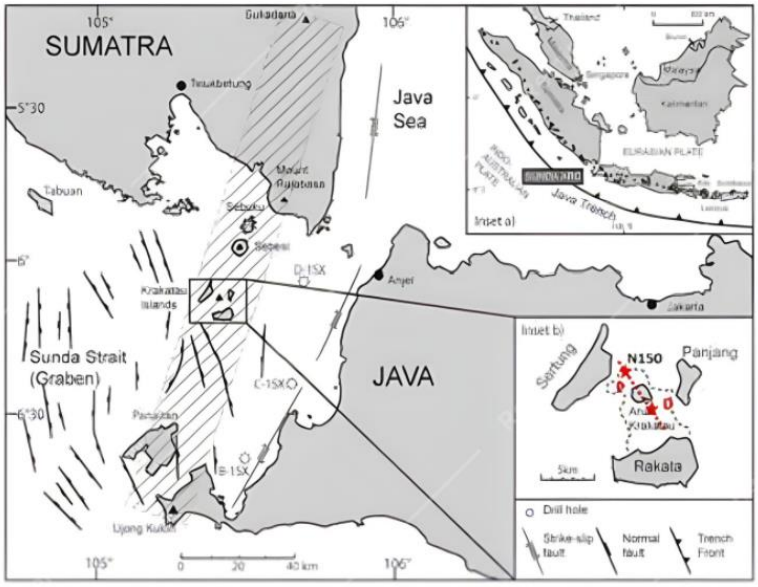

Figure 2. Geological framework of the Sunda Strait as an extensional tectonic zone (Tim Badan Geologi, 2019).

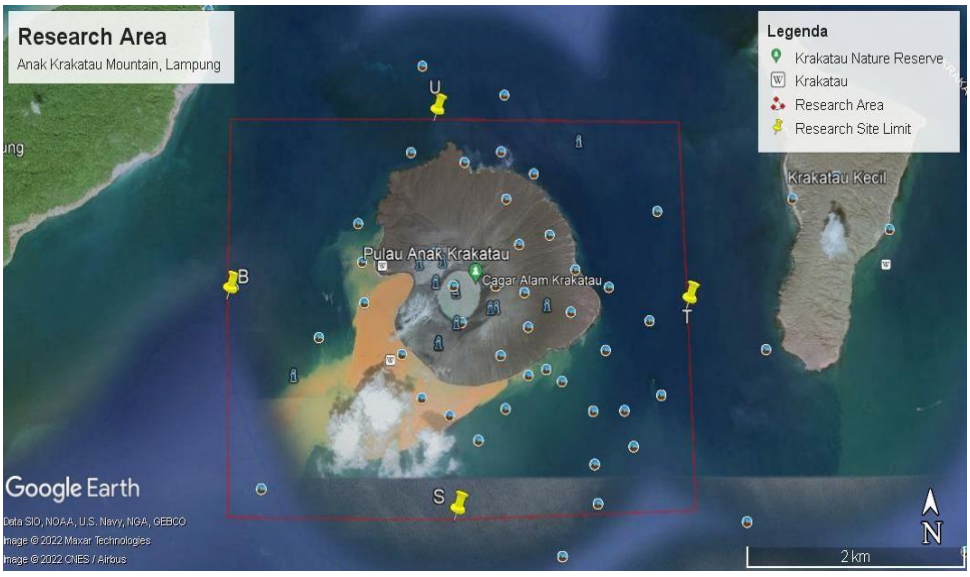

Figure 3. Research area map.

The gravity anomaly data obtained from satellite imagery represents the corrected gravitational acceleration, including free-air correction. Therefore, for analysis, terrain correction and Bouguer correction need to be applied to obtain the Complete Bouguer Anomaly (CBA) (Indriani et al., 2023). The Complete Bouguer Anomaly (CBA) values derived from corrections in satellite gravity data undergo upward continuation to separate regional and residual gravity anomalies (Utama, 2023). The gravity method was chosen because it can provide detailed information about the geological structure and density contrast of the rocks (Anggraeni, 2023). The data processing steps starting from data

acquisition to creating a 3D model of the subsurface structure of Mount Anak Krakatau can be seen in Figure 4.

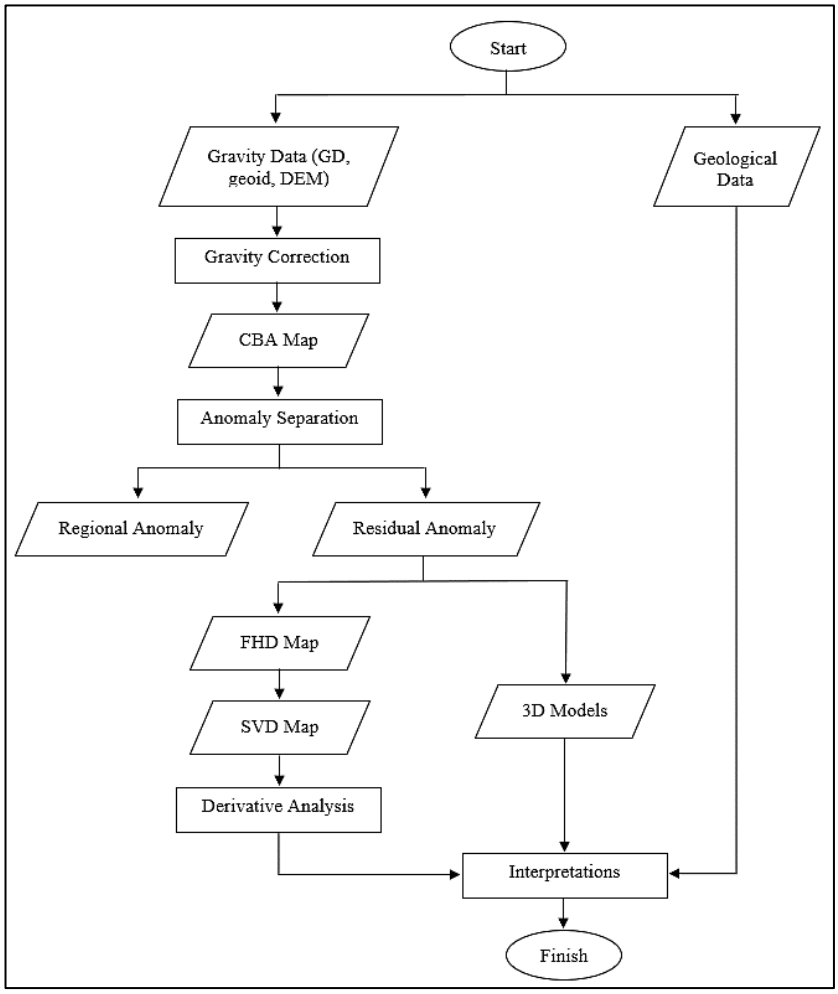

Figure 4. Research flowchart.

3. Results and Discussions

3.1 Complete Bouguer Anomaly (CBA)

The CBA map in Figure 5 shows that the distribution of gravity anomaly values in the research location ranges from 45 to 61.6 mGal. The low anomaly values in the southern part, ranging from 45 to 47.9 mGal, are believed to be associated with the sea zone. On the other hand, the high anomaly values, ranging from 55 to 61.6 mGal, extending from the north to the south, are believed to be associated with the elevation and caldera of Mount Anak Krakatau, as well as the rock formations consisting of porphyritic andesite and dacite (QTp). However, this CBA map still contains a mixture of residual (shallow) and regional (deep) anomalies. To eliminate ambiguity in further interpretation, the separation of regional and residual anomalies is conducted.

3.2 Regional and Residual Anomaly

After separating the anomalies, both regional and residual anomalies were obtained. On the regional anomaly map, the distribution of gravity anomaly values ranges from 45.4 to 62.2 mGal. This regional anomaly is caused by the response of rocks at considerable depths beneath the Earth's surface and

exhibits contour patterns similar to the CBA map. However, the regional anomaly map in Figure 6 has smoother contours compared to the CBA map.

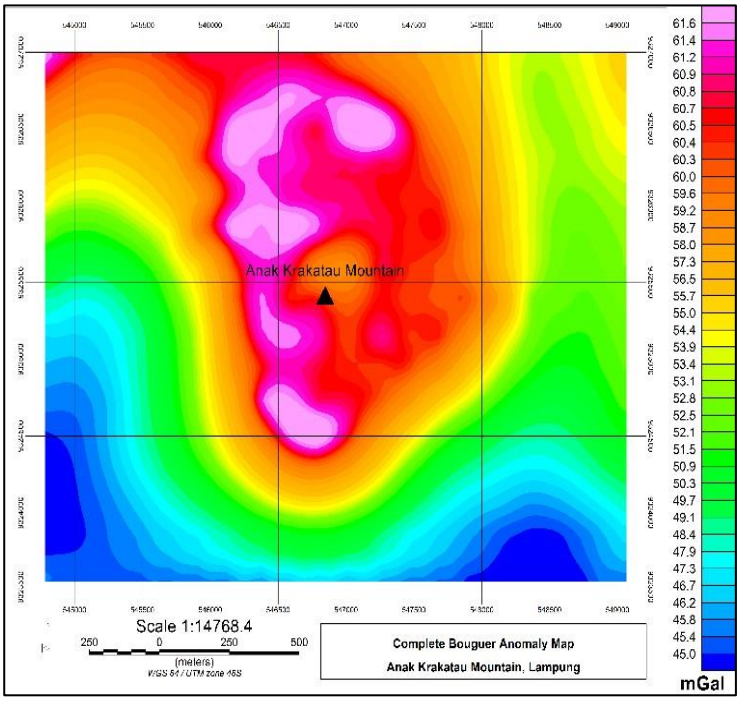

Figure 5. Complete bouguer anomaly map.

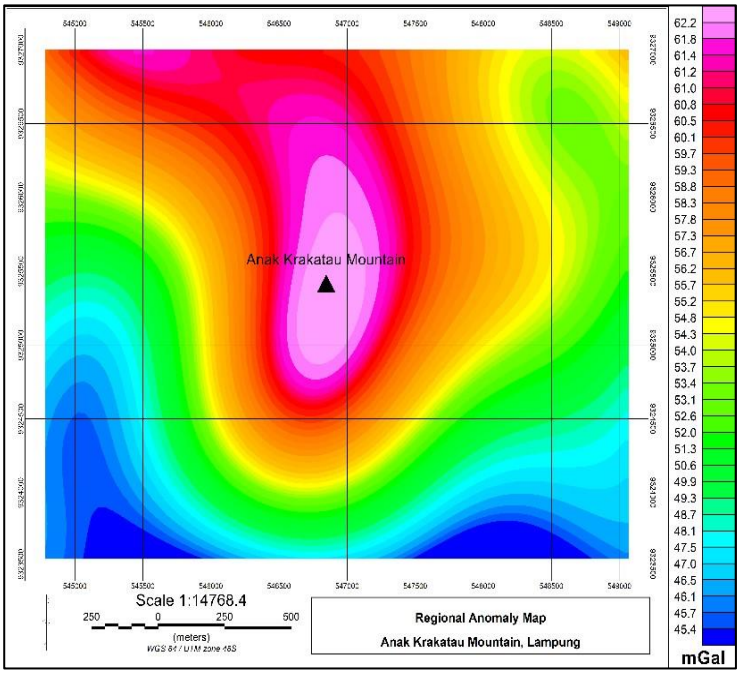

Figure 6. Regional anomaly map.

On the residual anomaly map in Figure 7, the distribution of gravity anomaly values ranges from -1.85 to 2.13 mGal. This residual anomaly is caused by the response of shallow rocks beneath the Earth's surface, and the map exhibits more varied or heterogeneous contour patterns. The low anomalies, located directly beneath Mount Anak Krakatau, have values ranging from 1.85 to -0.89 mGal, which are believed to be associated with magma pockets beneath Mount Anak Krakatau. The high anomalies surrounding Mount Anak Krakatau have values ranging from 0.04 to 2.13 mGal, and they are believed

to be associated with the caldera of Mount Anak Krakatau and the rock formations of porphyritic andesite and dacite (QTp). Subsequently, the residual anomaly map is cropped to match the location for further overlay and 3D modeling, as shown in Figure 7.

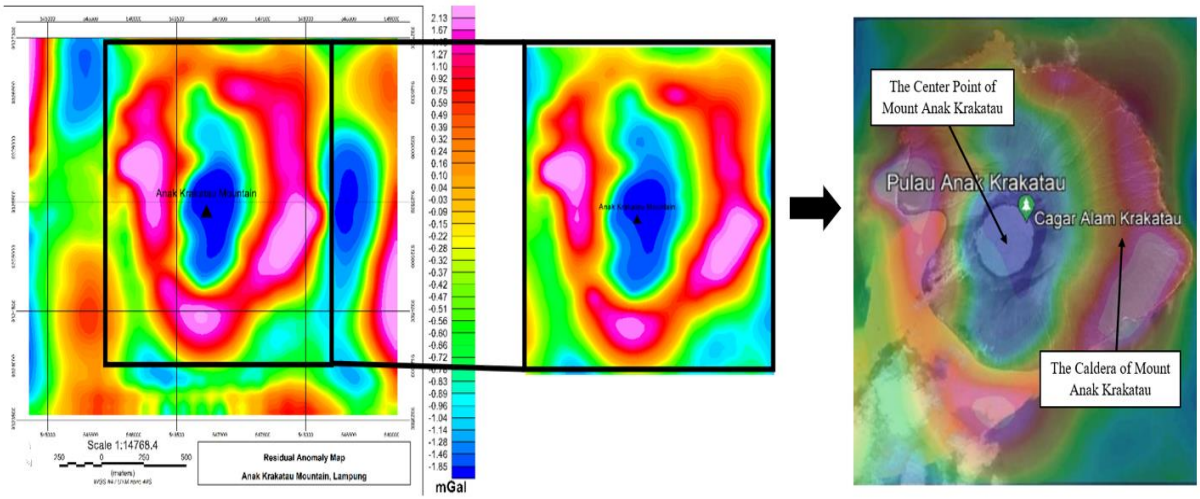

Figure 7. Overlay residual anomaly map and Google Earth.

3.3 Derivative Analysis

In this derivative analysis, the First Horizontal Derivative (FHD) and Second Vertical Derivative (SVD) filters are applied to determine the location and type of faults controlling the geothermal system in the Mount Anak Krakatau area. The characteristics of maximum FHD values and SVD values close to zero indicate the presence of faults. On the FHD map in Figure 8, anomalies are distributed within the range of 0.00073 to 0.01220 mGal. Among them, 16 geological structures, including the caldera of Mount Anak Krakatau, exhibit very high anomaly values ranging from 0.00810 to 0.01220 mGal. These structures control the geothermal system of Mount Anak Krakatau, with a dominant fault direction from northwest to southeast, as indicated by the black lines on the FHD map.

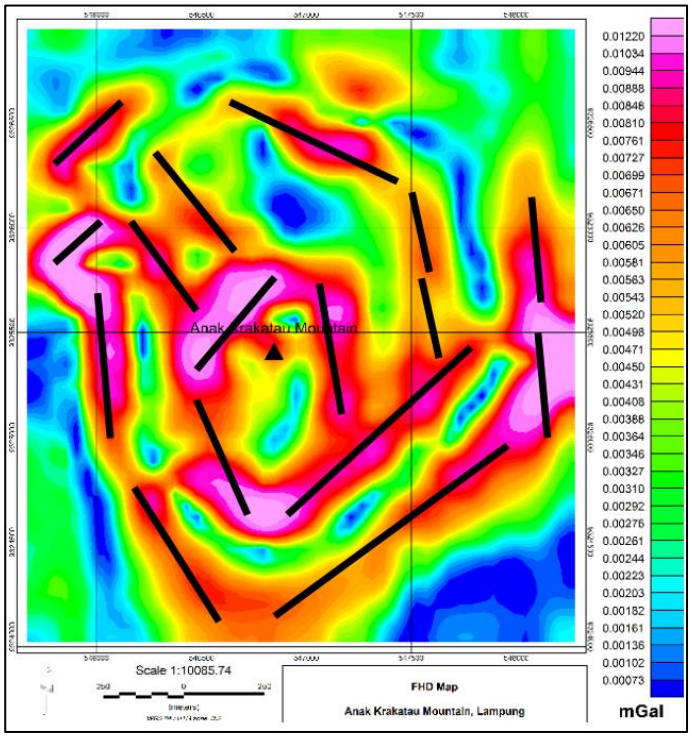

Figure 8. First Horizontal Derivative (FHD) Map.

On the SVD map in Figure 9, anomalies are distributed within the range of -0.0000960 to 0.0001216 mGal. There are 16 geological structures, including the caldera of Mount Anak Krakatau, with anomaly values close to 0 mGal (indicated by the transition of colors from green to yellow) that control the geothermal system of Mount Anak Krakatau. The dominant fault direction is from northwest to southeast, as indicated by the black lines on the SVD map.

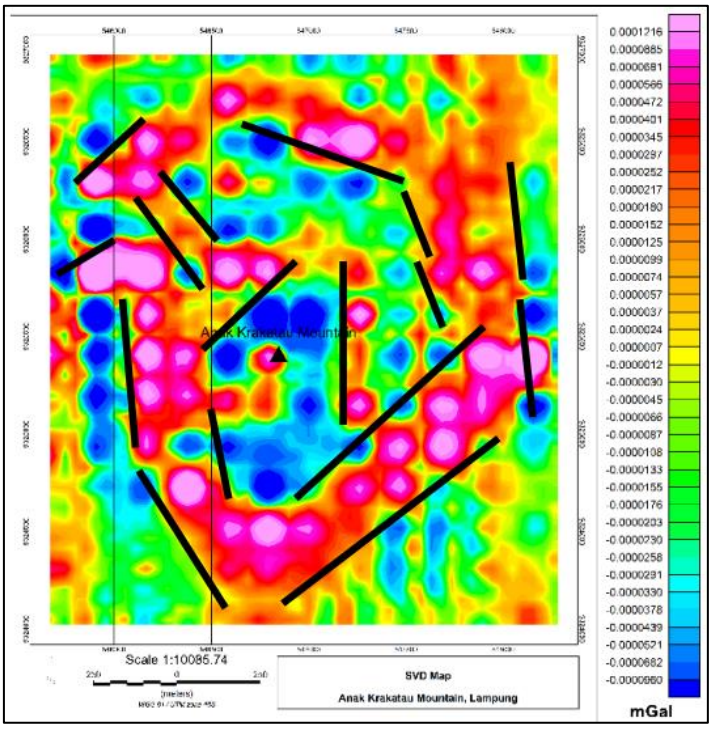

Figure 9. Second Vertical Derivative (SVD) Map.

To determine the type of faults controlling the geothermal system of Mount Anak Krakatau, section digitization is performed by cutting across the faults on the FHD and SVD maps to obtain the FHD and SVD curves for fault analysis. Five east-west sections are conducted, intersecting the faults around the research area (indicated by thin black lines) on the FHD and SVD maps, as shown in Figure 10.

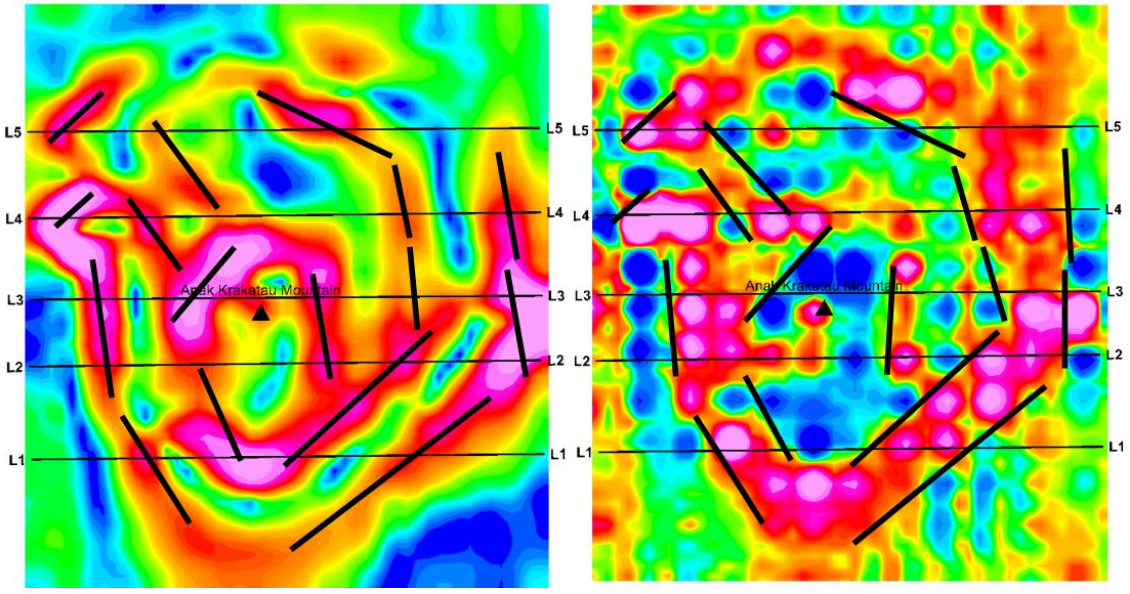

(a) (b)

Figure 10. Section map (a) FHD Map, (b) SVD Map.

In the results of the fault analysis in section 1 (L1) based on the normalized FHD and SVD curves, it is observed that there are two normal faults, namely F1 with coordinates (546255.7, 9324683) and F2 with coordinates (547605.7, 9324698) (Figure 11).

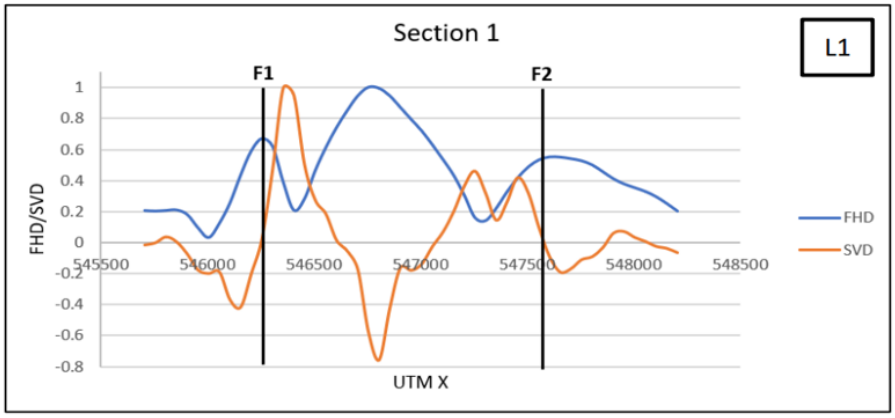

Name	UTM X	UTM Y	Max SVD	Min SVD	Fault Type
F1	546255.7	9324683	1	0.42	Normal
F2	547605.7	9324698	0.42	0.19	Normal

Figure 11. The fault analysis in section 1 (L1).

In the results of the fault analysis in section 2 (L2) based on the normalized FHD and SVD curves, it is observed that there are two normal faults and two reverse faults. In Figure 12, the normal faults are labeled as F1 with coordinates (546141.7, 9325145.7) and F3 with coordinates (547591.6, 9325163.4). The reverse faults are labeled as F2 with coordinates (547141.6, 9325157.9) and F4 with coordinates (548091.5, 9325169.5).

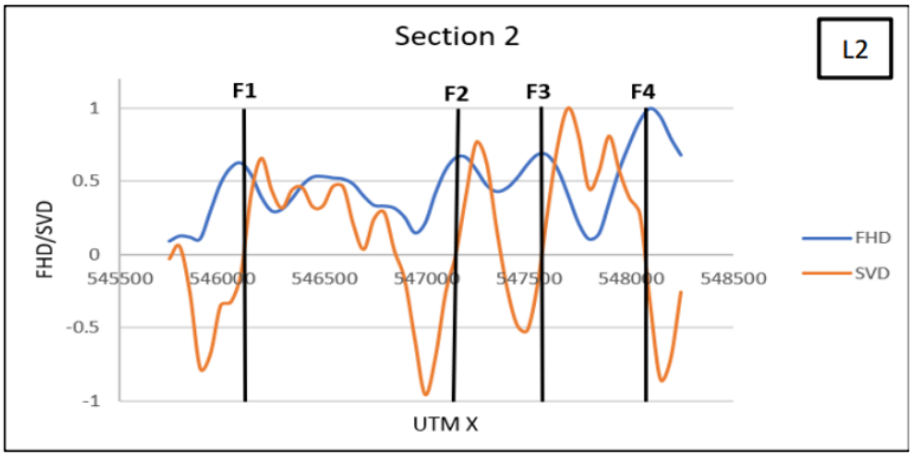

Name	UTM X	UTM Y	SVD Max	SVD Min	Fault Type
F1	546141.7	9325146	0.66	0.32	Normal
F2	547141.6	9325158	0.76	0.96	Reverse
F3	547591.6	9325163	1	0.52	Normal
F4	548091.5	9325170	0.8	0.85	Reverse

Figure 12. The fault analysis in section 2 (L2).

In the results of the fault analysis in section 3 (L3) based on the normalized FHD and SVD curves, Figure 13 shows that there are five reverse faults. The reverse faults are labeled as F1 with coordinates (546095.6, 9325476.8), F2 with coordinates (546545.6, 9325480.3), F3 with coordinates (547245.6,

9325485.6), F4 with coordinates (547545.6, 9325487.9), and F5 with coordinates (548195.6, 9325492.9).

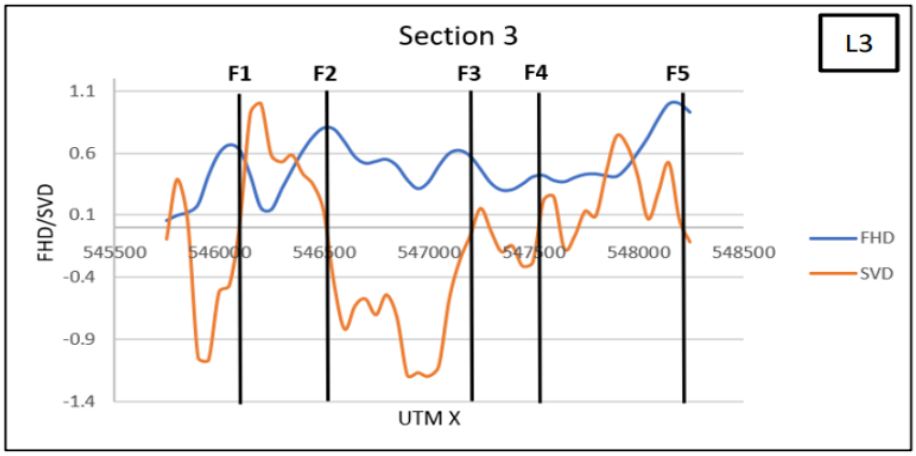

Name	UTM X	UTM Y	Max SVD	Min SVD	Fault Type
F1	546095.6	9325477	1	1.07	Reverse
F2	546545.6	9325480	0.58	0.82	Reverse
F3	547245.6	9325486	0.15	1.2	Reverse
F4	547545.6	9325488	0.2	0.3	Reverse
F5	548195.6	9325493	0.8	0.85	Reverse

Figure 13. The fault analysis in section 3 (L3).

In the results of the fault analysis in section 4 (L4) based on the normalized FHD and SVD curves, Figure 14 indicates that there are four normal faults. The normal faults are labeled as F1 with coordinates (545837.8, 9325879.8), F2 with coordinates (546337.7, 9325885.9), F3 with coordinates (547537.7, 9325900.6), and F4 with coordinates (548087.6, 9325907.3).

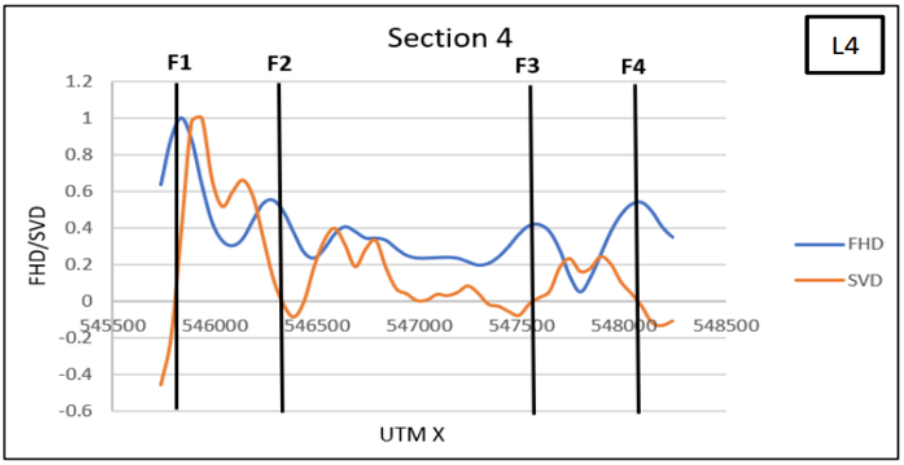

Name	UTM X	UTM Y	SVD Max	SVD Min	Fault Type
F1	545837.8	9325880	1	0.4	Normal
F2	546337.7	9325886	0.66	0.002	Normal
F3	547537.7	9325901	0.23	0.002	Normal
F4	548087.6	9325907	0.24	0.13	Normal

Figure 14. The fault analysis in section 4 (L4).

In the results of the fault analysis in section 5 (L5) based on the normalized FHD and SVD curves in Figure 15, it is observed that there are three normal faults. The normal faults are labeled as F1 with

coordinates (545833.9, 9326310.8), F2 with coordinates (546283.9, 9326314.2), and F3 with coordinates (548083.8, 9326327.8).

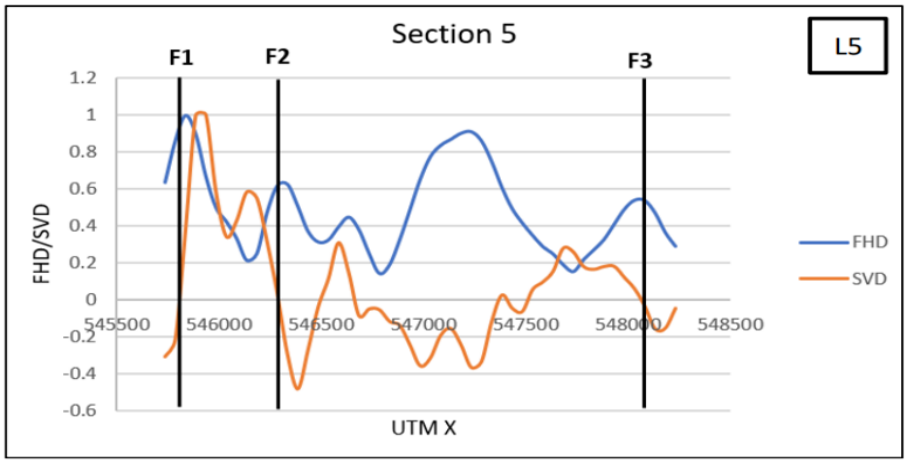

Name	UTM X	UTM Y	SVD Max	SVD Min	Fault Type
F1	545833.9	9326311	1	0.3	Normal
F2	546283.9	9326314	0.55	0.49	Normal
F3	548083.8	9326328	0.18	0.16	Normal

Figure 15. The fault analysis in section 5 (L5).

3.4 3D Inverse Modelling

In this stage, a 3D inversion modeling is performed to depict the subsurface structure of the geothermal system in the Mount Anak Krakatau region, correlated with the results of the FHD and SVD graph analyses to determine the faults controlling the geothermal system. In the model A-A' oriented from west to east, it can be observed that there is a clay cap layer with a depth range of 0 to 500 m and density values ranging from 2.32 to 2.37 g/cc. Below the clay cap layer, there is a reservoir layer consisting of porphyritic andesite and dacite, with a depth range of 500 to 1100 m and density values ranging from 2.23 to 2.29 g/cc. Additionally, two normal faults controlling the geothermal system are identified based on the correlation between the FHD and SVD, as shown in Figure 16.

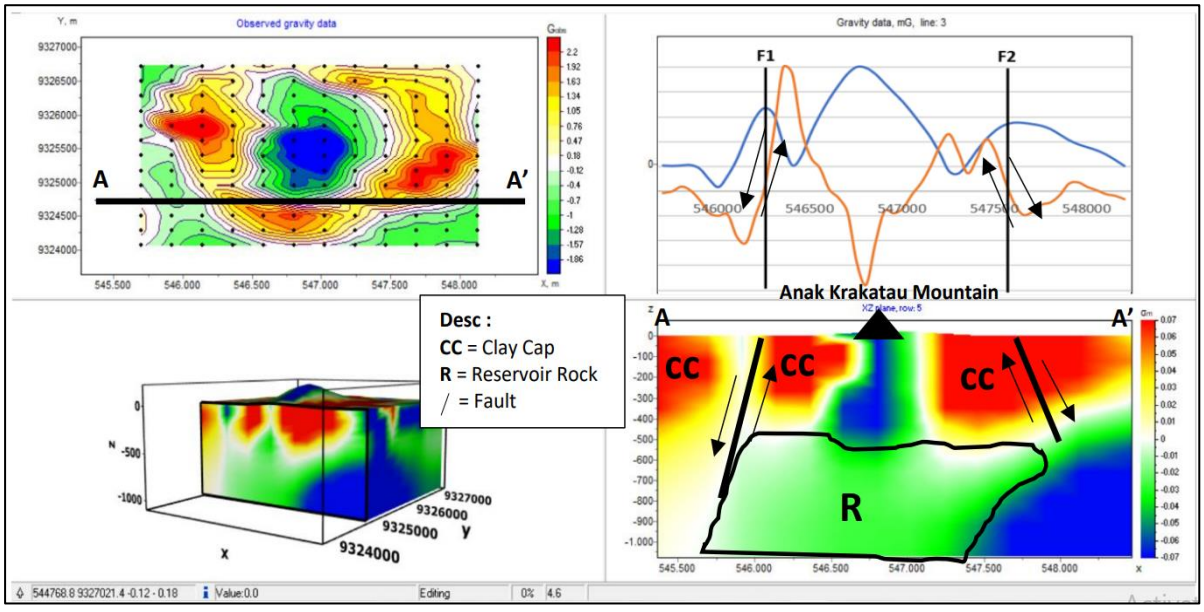

Figure 16. A-A’ section of 3D model.

In model B-B' oriented from west to east, similar to the previous model, there is a clay cap layer with a depth range of 0 to 500 m and density values ranging from 2.32 to 2.37 g/cc. Below the clay cap layer, there is a reservoir layer consisting of porphyritic andesite and dacite, with a depth range of 500 to 1100 m and density values ranging from 2.23 to 2.29 g/cc. Additionally, two normal faults and two reverse faults controlling the geothermal system are identified based on the correlation between the FHD and SVD (Figure 17).

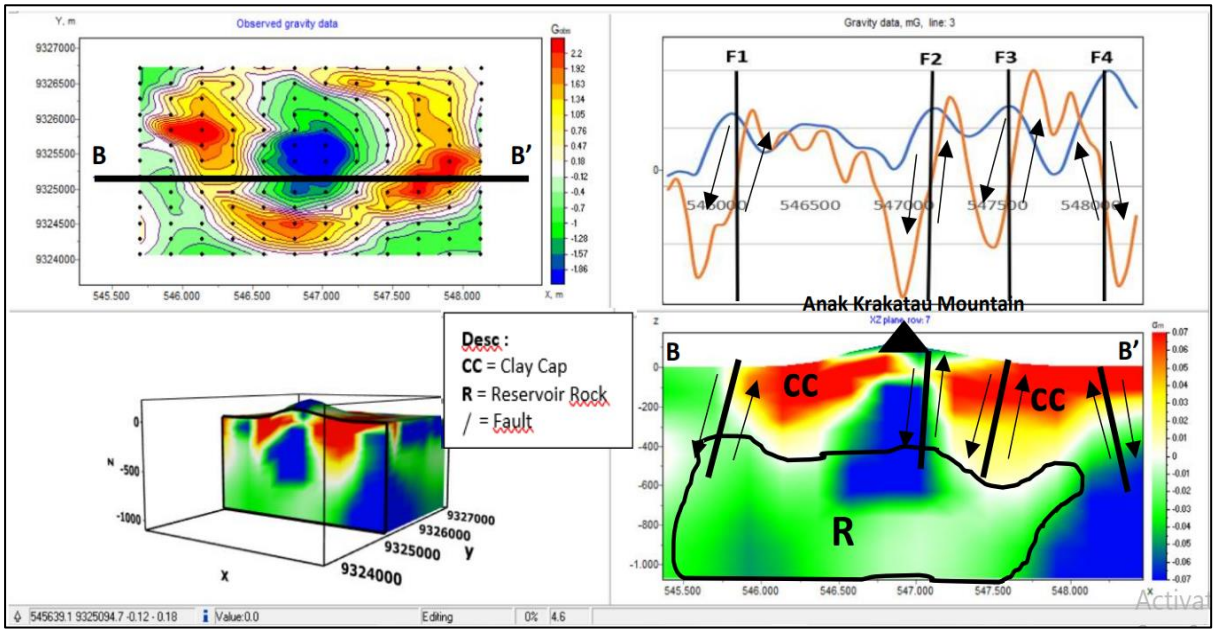

Figure 17. B-B' section of 3D model.

In model C-C' oriented from west to east, similar to the previous models, there is a clay cap layer with a depth range of 0 to 500 m and density values ranging from 2.32 to 2.37 g/cc. Below the clay cap layer, there is a reservoir layer consisting of porphyritic andesite and dacite, with a depth range of 500 to 1100 m and density values ranging from 2.23 to 2.29 g/cc. Additionally, five reverse faults controlling the geothermal system are identified based on the correlation between the FHD and SVD, as shown in Figure 18.

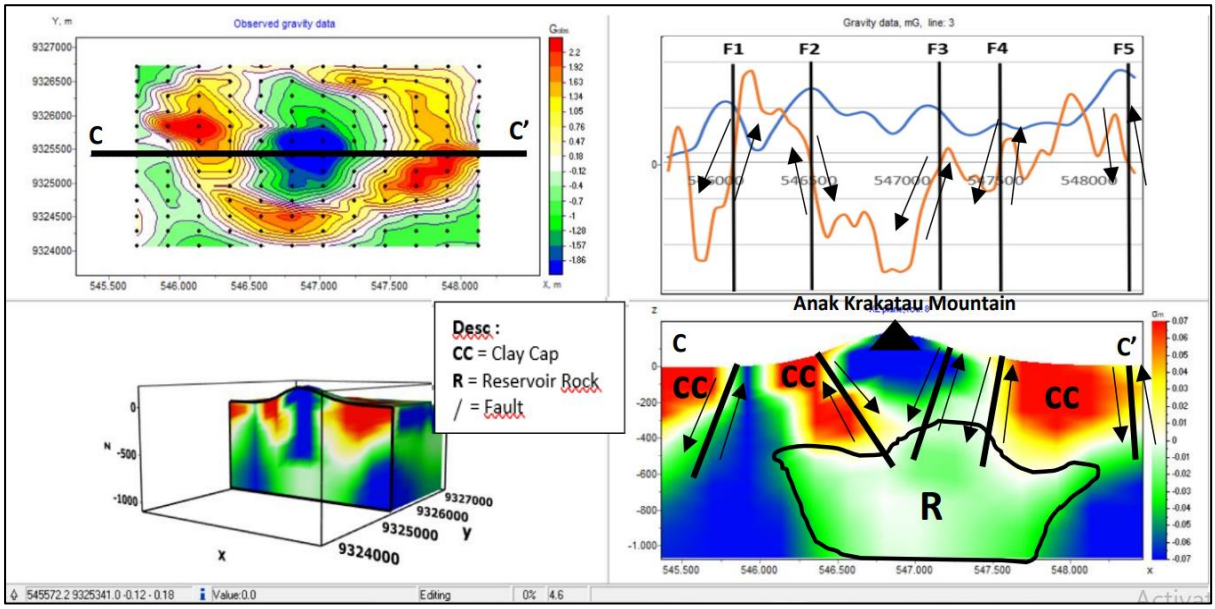

Figure 18. C-C' Section of 3D Model.

In model D-D' oriented from west to east, there is a clay cap layer with a depth range of 0 to 600 m and density values ranging from 2.32 to 2.37 g/cc. Below the clay cap layer, there is a reservoir layer consisting of porphyritic andesite and dacite, with a depth range of 500 to 1100 m and density values ranging from 2.23 to 2.29 g/cc. Additionally, four normal faults controlling the geothermal system are identified based on the correlation between the FHD and SVD (Figure 19).

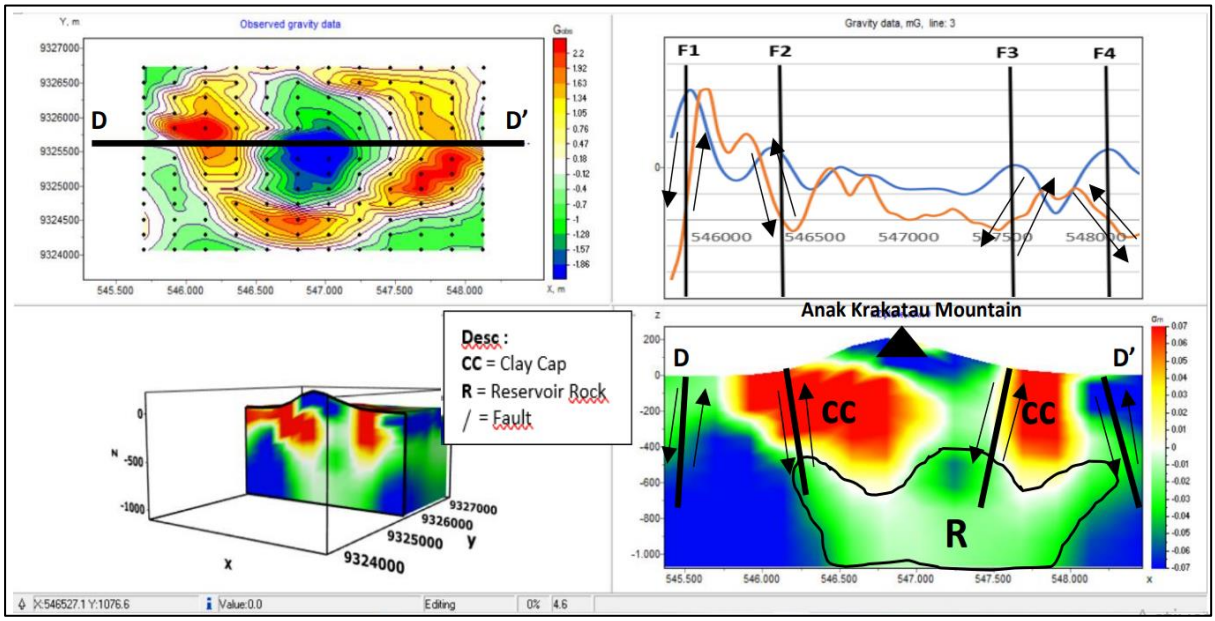

Figure 19. D-D’ section of 3D model.

In model E-E' oriented from west to east, there is a clay cap layer with a depth range of 0 to 600 m and density values ranging from 2.32 to 2.37 g/cc. Below the clay cap layer, there is a reservoir layer consisting of porphyritic andesite and dacite, with a depth range of 500 to 1100 m and density values ranging from 2.23 to 2.29 g/cc. In Figure 20, three normal faults controlling the geothermal system are identified based on the correlation between the FHD and SVD.

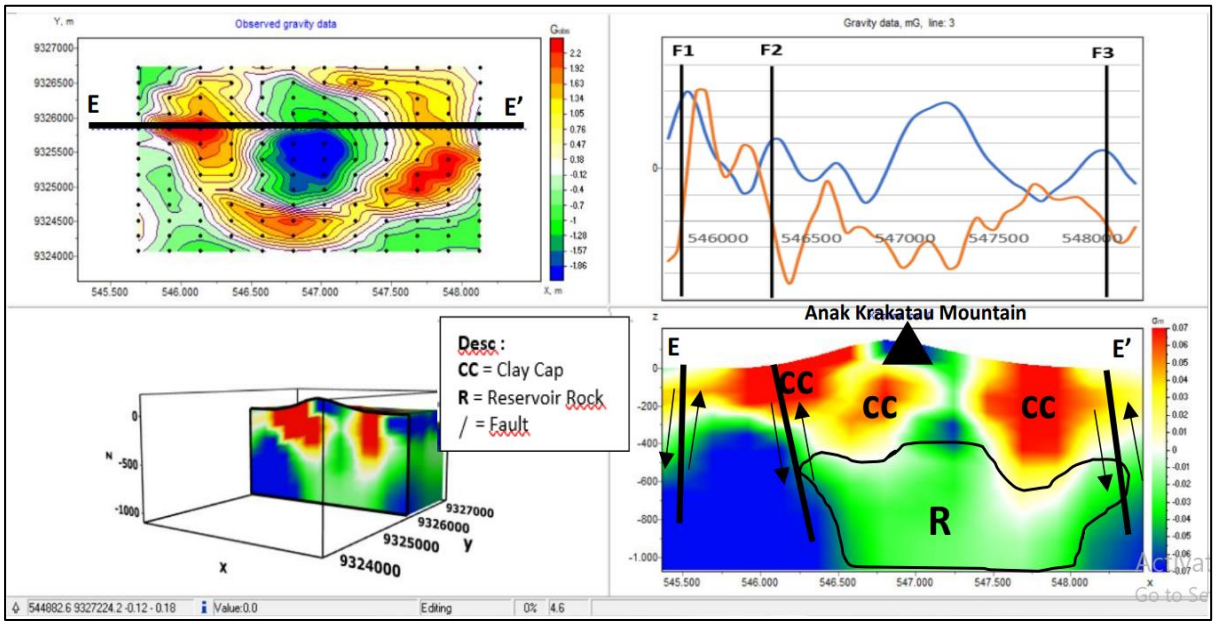

Figure 20. E-E’ section of 3D model.

4. Conclusions

Based on the analysis of the residual anomaly map, the low anomalies beneath Mount Anak Krakatau have values from -1.85 to -0.89 mGal, which are suspected to be associated with the magma chamber beneath the volcano. Meanwhile, the high anomalies with values from 0.04 to 2.13 mGal are suspected to be associated with the Caldera of Mount Anak Krakatau and its constituent rocks, namely porphyritic andesite and dacite (QTp). Based on the analysis of the FHD and SVD graphs, a total of 18 faults were identified as controlling the geothermal system in the Mount Anak Krakatau region, comprising nine normal faults and nine reverse faults. Based on the results of the section from the 3D modeling oriented from west to east, it is evident that the Mount Anak Krakatau region has a clay cap layer with an average depth of 0 to 550 m and density values from 2.32 to 2.37 g/cc. Below the clay cap layer, there is a reservoir layer consisting of porphyritic andesite and dacite, with a depth range of 500 to 1100 m and density values from 2.23 to 2.29 g/cc.

The authors hope that in the future, this gravity method will be updated and will become more sophisticated so that it is widely used in Indonesia for the geothermal energy sector and also that the government will pay more attention to geothermal energy, where geothermal energy is very large in Indonesia (40% of world reserves) so that Indonesia is a country that is clean from pollution and can reduce dependence on coal energy which has high carbon emissions.

Acknowledgment

The authors would like to thank GeoXplore Indonesia and PT Minelog Services Indonesia for supporting and providing facilities for this research.

References

Anggraeni, F. K., Astutik, S., Nurlyan, M. R., Utami, R. D., Putri, O. Z., & Maudina, D. (2023). Identifikasi struktur bawah permukaan Gunung Semeru pasca erupsi tahun 2022. *Jurnal Ilmu dan Inovasi Fisika*, *7*(1), 69–77.

Ariyanti, O. & Fattah, R.M. (2020). The process of establishing and activities of the Anak Krakatau Mountain. *Geographica: Science & Education Journal*, *2*(1), 46–54.

Aufia, Y. F., Karyanto, and Rustadi. (2019). Pendugaan patahan daerah "Y" berdasarkan anomali gaya berat dengan analisis derivative. *Jurnal Geofisika Eksplorasi*, *5*(1), 75–88.

Buijze, L, et al. (2019). Review Of induced seismicity in geothermal systems worldwide and implications for geothermal systems in the Netherlands. *Netherlands Journal of Geosciences*, *98*(13). https://doi.org/10.1017/njg.2019.6

Camacho, M., & Alvarez, R. (2021). Geophysical modeling with satellite gravity data: Eigen-6C4 vs. GGM Plus. *Engineering*, *13*(12), 690706. https://doi.org/10.4236/eng.2021.1312050

Citraningrum, Y. P., et al, (2023). Subsurface interpretation of the Sembalun Area, East Lombok using the gravity method. *Cognizance Journal of Multidisciplinary Studies*, *3*(11), 1–8.

Cordell, L. (1979). Gravimetric expression of graben faulting in Santa Fe Country and the Espanola Basin, New Mexico. Guidebook to Santa Fe Country. In: *Ingersoll, R.V., Ed., New Mexico* Geological Society Guidebook: 30th Field Conference, 59–64.

Dewi, C. N., Maryanto, S., & Rachmansyah, A. (2015). Sistem panasbumi daerah Blawan, Jawa Timur berdasarkan survei magnetotelurik. *Jurnal RISET Geologi dan Pertambangan*, *25*(2), 111–119. https://doi.org/10.14203/risetgeotam2015.v25.262

Firdaus, A., Harmoko, U., & Widada, S. (2014). Pemodelan steady state sistem panas bumi daerah sumber air panas Diwak-Derakan dengan menggunakan software hydrothrem 2.2. *Youngster Physics Journal*. *3*(4), 243–250.

Fitriani, D. S., Putri, S. N. A., & Putrajy, I. F. (2020). Metode gravitasi untuk identifikasi Sesar Weluki dengan analisis first horizontal derivative dan second vertical derivative. *Prosiding Seminar Nasional Fisika (SNF), IX*, 53–60. https://doi.org/10.21009/03.SNF2020.01.FA.10

Gunawan, B., Anjani, A., & Anjalni, A. (2022). Identifikasi pemodelan 2d dan suhu permukaan daerah panas bumi Gunung Gede-Pangrango, Jawa Barat menggunakan metode gravitasi. *Journal of Engineering Environmental Energy and Science*, *1*(1), 1–14.

Hirt, C., Claessens, C., Fecher, T., Kuhn, M., Pail, R., & Rexer, P. (2013). New ultra-high resolution picture of 2 Earth's gravity field. *Geophysical Research Letters*, *40*, https://doi.org/10.1002/grl.50838

Indriani, R. F., Anjasmara, I. M., Utama, W., Rafi, M. E. D., & Gaol, D. J. L. (2023). Geological structure model for recharge area in Patuha Geothermal Field. *IOP Conf. Series: Earth and Environmental Science*. 1276 012052. https://doi.org/10.1088/1755-1315/1276/1/012052

Nafian, M., Gunawan, B., & Permana. N.R. (2021). 2D forward modeling geothermal system gravity data in South Solok Region, West Sumatra. Al-Fiziya. *Journal of Materials Science, Geophysics, Instrumentation and Theoretical Physics*, 36–44.

Perwita, C. A., Maryanto, S., Ghufron, M., Prakoso, M., Abigail, S., & Zamhar, U. Z. N. (2020). Korelasi peningkatan temperatur permukaan tanah dan aktivitas seismik di Gunung Anak Krakatau pada tahun 2018. *Jurnal Lingkungan dan Bencana Geologi*, *11*(3), 135–142.

Putra, P. S. & Yulianto, E. (2017). Karakteristik endapan tsunami krakatau 1883 di daerah Tarahan, Lampung. *Jurnal RISET Geologi dan Pertambangan*, *27*(1), 83–95.

Rachmawati, F. A., Haryanto, A. D., Hutabarat, J., & Sumaryadi, M. (2019). Penentuan sumber panas sistem panas bumi Gunung Api Talang, Sumatera Barat berdasarkan sejarah panas dan geokimia air. *Padjajaran Geoscience Journal*, *3*(1), 44–50.

Raharjo, S. A., Saputra, A. V., & Rahadinata, T. (2022). Identifikasi struktur geologi bawah permukaan berdasarkan pemodelan 3D data gravitasi (studi kasus daerah potensi panas bumi Kepahiang). *Jurnal Teras Fisika*, *5*(2), 28–35. https://doi.org/10.20884/1.jtf.2022.5.2.7248

Ramadhan, A. B., Djayus, D., & Lepong, P. (2020). Analisa struktur bawah permukaan daerah prospek panas bumi "GF-TNH" Sumatera Barat berdasarkan metode gaya berat. *Jurnal Geosains Kutai Basin*, *3*(1), 1–10. https://doi.org/10.30872/geofisunmul.v3i1.594

Rizkiani, D. N., & Rustadi. (2019). Interpretasi sistem panas bumi Suwawa berdasarkan data gaya berat. *Jurnal Geofisika Eksplorasi*, *5*(2), 42–52.

Saad, S. N., (2022). *Studi geokimia batuan gunung api Anak Krakatau hasil erupsi Desember 2018*. Universitas Hasanuddin.

Sigfússon, B., & Uihlein, A. (2015). *Technology, market and economic aspects of geothermal energy in Europe.* The European Union.

Sumintadireja, P. (2012). *GL3142: Volkanologi dan geotermal*. Penerbit ITB.

Suprianto, A., Supriyadi., Priyantari, P., & Cahyono., B. E. (2021). Correlation between GGMPlus, Topex and BGI gravity data in volcanic areas of Java Island. *Journal of Physics: Conference Series*. 1825 012023. https://doi.org/10.1088/1742-6596/1825/1/012023

Sutawidjaja, I. S. (2006). Pertumbuhan Gunung Api Anak Krakatau setelah letusan katastrofis 1883. *Jurnal Geologi Indonesia*, *1*(3), 143–153.

Syafawi, I., Suhendi, C., & Yudistira, T. (2015). *Identifikasi tubuh magma Gunung Api Anak Krakatau berdasarkan struktur kecepatan seismik 3D menggunakan tomografi gempa lokal*. Institut Teknologi Sumatera.

Telford, W. M., Eldart, L. M., & Sheriff, R. E. (2004). *Applied geophysics* (2nd Edition). Cambridge University Press.

Tim Badan Geologi. (2019). *Dinamika geologi Selat Sunda dalam pembangunan berkelanjutan*. Badan Geologi, Kementerian Energi dan Sumber Daya Mineral.

Utama, W., Putra, D. P. N., Garini, S. A., & Indriani, R. F. (2023). Optimizing surface lithology interpretation from global gravity model and landsat 8 satellite imagery in Semeru Mountain, Indonesia. *IOP Conf. Series: Earth and Environmental Science*. 1276 012048. https://doi.org/10.1088/1755-1315/1276/1/012048